PN-ACL-675

Slags & mattes in Vanyukov's process for the extraction of copper

S. Vaisburd[1], A. Berner[1], D.G. Brandon[1], S. Kozhakhmetov[2], E. Kenzhaliyev[2], R. Zhalelev[2]

[1]Faculty of Materials Engineering, Technion – Israel Institute of Technology, Haifa 32000, Israel

[2]Institute of Metallurgy and Ore Beneficiation, Almaty 480100, Kazakstan

ABSTRACT

Slags and matte in Vanyukov's process, an autogeneous method of processing sulfide concentrates of non-ferrous metals used in a specially designed furnace at the Balkhash copper-smelting plant (Kazakstan), have been characterized by scanning electron microscopy, energy dispersive spectroscopy and X-ray diffraction. The liquid matte was shown to have contained 3.6 wt pct of slag inclusions and about 4 wt pct of magnetite. The solid matte is a mixture of sulfide phases. The liquid waste slag was shown to have contained 0.6 wt pct of matte inclusions and about 3 wt pct of magnetite. The silicate field of the solid slag consists of two phases, identified as iron orthosilicate and iron metasilicate. It was shown that most slag formation occured before the over-current stage of the process. Metal losses in the slag were found to take three forms: mechanical (matte inclusions entrained in the liquid slag), chemical (metal oxide formation) and physical (metal sulfides dissolved in the liquid slag). Thermodynamic calculation of the exchange reactions for the oxide and sulfide components of the slag showed that zinc and lead dissolved in the slag are present mainly as chemical losses but with only a small part (10-20 pct) in the form of physical losses. By contrast, copper losses occur only as mechanical and physical

losses. The results of these thermodynamic calculations are supported by the experimental data.

Slags & mattes in Vanyukov's process for copper extraction

S. Vaisburd[1], A. Berner[1], D.G. Brandon[1], S. Kozhakhmetov[2], E. Kenzhaliyev[2], R. Zhalelev[2]

[1]Faculty of Materials Engineering, Technion – Israel Institute of Technology, Haifa 32000, Israel

[2]Institute of Metallurgy and Ore Beneficiation, Almaty 480100, Kazakstan

I. INTRODUCTION

Vanyukov's process of copper extraction is an autogeneous method for sulfide concentrates of non-ferrous metals present in a liquid matte-slag emulsion. Melting is accomplished in a specially designed furnace for the continuous counter-flow of matte and slag melts during the reaction [1]. The most prominent features of this method are: (1) high productivity (2.1-3.3 $ton \cdot m^{-2} \cdot h^{-1}$); (2) low dust loss (about 1 pct of the charge weight); (3) possible charge processing without complete drying (up to 6-8 pct moisture); (4) possible processing of lump materials (down to 50 mm). Vanyukov's process has been put in production at some metallurgical plants in Russia and Kazakstan, but the slags and mattes formed have not been extensively studied. The primary purpose of the present research was to analyze the chemical and phase composition of slag and matte and determine the metal losses in the slags. In the present paper we present data from the Balkhash mining-metallurgical plant. For additional technological details the reader is referred to Ref. [1, 2].

II. EXPERIMENTAL

A. Materials

Samples of slags and matte were obtained from Vanyukov's furnace at the Balkhash mining-metallurgical plant. Slag samples were taken at the end of the process (waste slag) and from the over-current zone. The over-current is the region in Vanyukov's furnace where the slag is released from the melting zone into the electrothermic settling tank [1]. The results of chemical analysis of the samples are given in Table I.

B. Sample preparation

Sections were cut from the samples using a diamond wheel before being mounted in epoxy resin. The sections were ground sequentially on 240, 320, 400 and 600 grit silicon carbide papers and polished with 3 and 1 μm alumina. For scanning electron microscopy and energy dispersive spectroscopy the specimens were subsequently carbon coated to ensure electrical conductivity.

C. Scanning Electron Microscopy (SEM) and Energy Dispersive Spectroscopy (EDS).

Phase and elemental analysis of the specimens using SEM and EDS was conducted on an XL30 (Philips, Holland) scanning electron microscope equipped with a LINK ISIS (Oxford Instruments, England) energy dispersive spectrometer. The measurements were performed at an accelerating voltage of 20 kV, a probe current of 1 nA and a working distance of 10.5 mm. Under these analytical conditions the probe

diameter on the sample surface was about 100 nm. The morphology of the different phases at the sample surface was imaged using back-scattered electrons in compositional contrast mode. After imaging in scanning mode, the electron probe was positioned sequentially at specific points on the sample surface and EDS spectra were collected. The take off angle for x-ray radiation collection was 35° and the spectra acquisition time was set at 100 s. In all cases the standard deviation of the measured intensity in a single measurement did not exceed 5 pct. Quantitative microanalysis was performed using the conventional ZAF correction procedure included in the LINK ISIS software. The final results were normalized to 100 pct. In order to analyze quantitatively small sub-micron particles directly a correction technique was used specially developed for this type of analysis [3, 4].

D. X-Ray Diffraction (XRD) Analysis.

XRD spectra were obtained with the Bragg-Brentano focusing scheme in a Philips Analytical PW3020 powder diffractometer at 40 kV and 40 mA. Diffraction patterns were acquired from polished samples in a step mode with 0.02° steps (2) and 4 s per point over diffraction angles from 20° to 90°.

III. RESULTS

A. Matte

Typical SEM images obtained from the polished surface of the matte specimen are presented in Fig.1. The complex contrast is inherent in a multiphase structure. The EDS spectra were collected from different positions on the sample surface marked by numbers 1-22 in Fig.1. The results of quantitative X-ray microanalysis are shown in Table II. The structure consists of various sulfides, oxides and reguli of metal alloys. The average compositions determined for the major constituent phases are presented

in Table III, and the XRD spectrum taken from this sample is shown in Fig.2. The interpretation of the XRD data is complicated by peak overlap due to the presence of a large number of multielement phases. Most peaks in the XRD spectrum can be attributed to three sulfide phases: Cu_8S_5 (Geerite; JCPDS, Standard Diffraction Pattern, # 33-0491 [5]), ZnS (Sphalerite, JCPDS, #. 05-0566) and PbS (Galena, JCPDS, # 05-0592). Slight discrepancies between the measured and the standard peak positions can be explained by atomic substitution of different metals (Cu, Fe, Zn, and Pb) for the specified metal atom in the standard chemical formulae. The XRD results are in agreement with the results of chemical analysis for the major phases (Table III). For example, the sulfide phase, which is a major component (more than 85 pct), is in our case $(Cu_{0.76}Fe_{0.24})_8S_5$ rather than Cu_8S_5. The rest of peaks in the XRD spectrum can be attributed to diverse sulfides (CuS, (Cu, Fe, Pb)S, FeS_2, $Cu_{1.92}S$) and magnetite (Fe_3O_4), which were also observed in the sample point analyses using EDS.

B. Slag from the over-current zone

A typical morphology of the sample surface is shown in Fig.3. The major part of the surface consists of the dark dendritic background. Two additional phases are observed as grey rectangular or trapezoid 5-15 μm particles and white coarse (1-7 μm) or fine (up to 1 μm) oval interdendritic particles. Area measurements showed that the relative surface fractions of these phases are approximately 94.3 pct, 5.5 pct and 0.2 pct, respectively. Some fields of view also contained large particles (several hundreds of micrometers), with a morphology similar to that of the matte sample (see, Fig.4). The results of EDS analysis from different positions in these large particles clearly show that these macro-particles consisted of phases characteristic of the matte sample. We conclude, that the macro-particles are matte mechanically entrained in the slag during the melting process.

The results of EDS analysis averaged over many points for each phase present in the sample are listed in Table IV, and the XRD spectrum taken from this sample is shown in Fig.5. All diffraction peaks in the XRD spectrum can be attributed to just two phases: (Fe, $Mg)_2SiO_4$ (Fayalite magnesian; JCPDS, # 07-0158) and Fe_3O_4 (Magnetite, JCPDS, # 19-0629). Some peaks could be attributed alternatively to a phase of $FeSiO_3$ (Clinoferrosilite, JCPDS, #17-0548) but strong overlap between all peaks of this phase with peaks of (Fe, $Mg)_2SiO_4$ makes unambiguous interpretation impossible. The EDS results support this interpretation. The chemical composition of the dendrites is in good agreement with the composition of iron orthosilicate Fe_2SiO_4, with iron partially replaced by different cations (Zn, Al, Mg, K, Ca, and Ba). The chemical composition of the interdendritic regions is close to that for iron metasilicate $FeSiO_3$. The slight difference in contrast between the dendrites and the interdendritic regions depends mainly on the iron content with the higher iron concentration giving the lighter contrast. The chemical composition of the grey rectangular or trapezoid particles corresponds to that of magnetite Fe_3O_4, which agrees with the XRD results. White coarse and fine oval particles of the third phase, whose small volume fraction (less than 1 pct) cannot contribute to the XRD pattern were found to be sulfides: mainly (Cu, Fe)S. The mean chemical composition of these particles, averaged over 30 particles, is close to that of the (Cu, $Fe)_8S_5$ phase, which is the major component of the matte (see Table III). Several sulfide particles had compositions, which deviated significantly from the mean composition. In particular, many particles corresponding to ZnS, (Cu, Fe, Zn)S, (Pb, Cu, Fe)S and (Cu, Fe, Zn, Pb)S were also observed.

C. Waste slag formed at the end of the process

A typical morphology of the sample surface is shown in Fig.6. As in the slag from the over-current zone, most of the surface consists of the dark dendritic background. The two other phases present are grey dendrites or rectangular and trapezoid particles and white coarse or fine oval particles. Large macro-particles of the matte were not found. Areal measurements showed that the relative surface fractions of the observed phases are approximately 96.0 pct, 3.5 pct and 0.8 pct, respectively. These results correspond closely to those for the sample of slag from the over-current zone. No difference between the XRD spectra from these two slags could be detected. The average results of EDS analysis over many points for each phase are listed in Table V. Again the major constituent phases in these two slags have similar chemical compositions.

IV. DISCUSSION

A. Matte

The solid matte contains two types of oxide inclusion: magnetite, which was dissolved in the liquid matte and precipitated during cooling, and slag inclusions that were present in the liquid matte as a dispersed phase. In order to calculate the chemical composition of the slag inclusions in the matte one can use the known fact that silica is insoluble in the sulfide melt. It follows that any silica observed in the matte composition must originate from one of the slag oxides. The ratios of the contents of all oxides to the silica content in the slag were derived from the chemical analyses (Table I, row 3) and were then used to calculate the contents of other slag oxides in the matte. These data are given in Table VI (row 1). Note that the CaO concentration calculated in this way coincides, within experimental error, with that

determined in the matte by chemical analysis (see Table I), which further confirms the above calculation method since calcia like silica is insoluble in the matte. The total content of slag inclusions in the matte is 3.6 wt pct. The average chemical composition of the slag inclusions was calculated by normalizing the data to 100 pct (Table VI, row 2). For comparison, Table VI also gives the mean composition of the slag inclusions in the matte determined by EDS (row 3) and the slag composition determined by chemical analysis (row 4). The agreement is satisfactory and the discrepancies can be explained by errors in the analysis data and the presence in the slag of some oxides (K_2O, BaO, Na_2O, MgO, and TiO_2), which were not determined by chemical analysis.

The matte composition is given in Table VII, where the atomic fractions of Fe, Cu, Zn and Pb have been transformed to the corresponding sulfide contents. The matte can only consist of the lowest sulfides (that is, Cu_2S, FeS, PbS and ZnS) [6]. According to the present results the sulfide, which occupies more than 85 pct of the matte volume, has the crystal structure of geerite (Cu_8S_5 or $3Cu_2S{\cdot}2CuS$). Atoms of Cu^{II} in this sulfide should be replacable by atoms of Fe^{II}, Zn^{II} or Pb^{II}, so that this sulfide should have a composition $(Cu_{0.75}Me_{0.25})_8S_5$, where Me denotes a sum of the Fe, Zn and Pb. This corresponds exactly with the mean chemical composition of the sulfide determined by EDS (see Table III).

Some deficiency of sulfur in the matte was noted and was attributed to metallization of the matte by copper. This metallization was also confirmed by the SEM/EDS results (see Fig.1, where metal reguli (Cu and AgCu) are clearly visible in the matte). Although the Cu–S system has a tendency to exfoliate in the liquid state, even at low sulfur depletion [7], the presence of other metals in the matte prevents separation of a metallic phase in the liquid state, and the observed metallic phases are

a result of liquation during cooling. The residue of 4.4 wt pct should be apparently assigned to magnetite, which is contained in the matte but was not determined by the chemical analysis, although the SEM/EDS results clearly demonstrate the presence of magnetite in the matte. Another possibility is the presence of oxygen dissolved in the melt, which also was not determined. The normalized matte composition is given in Table VII, row 2. The content of copper in the matte is higher, and of iron and sulfur lower, than their contents in mattes produced by conventional technologies [8, 9]. This is a characteristic feature of an autogeneous process where melting is achieved at higher oxygen potentials.

B. Slag

The SEM/EDS data show that the silicate field of the solidified slag consists of two interpenetrating phases, gray and black. The crystal structure and chemical composition of the grey phase corresponded to iron orthosilicate where iron was partially replaced by several different cations (Zn, Mg, Ca, and Ba). The relatively low iron content (16.1 atomic pct instead of 28.6 atomic pct expected from the stoichiometry of Fe_2SiO_4) could explain why this phase crystallized as fayalite magnesian $(Fe, Mg)_2SiO_4$ instead of Fe_2SiO_4. The structure and chemical composition of the black phase corresponds to iron metasilicate. The results of chemical analysis presented in Table I support this interpretation: the silica concentration in the liquid slag is about 34 wt pct intermediate between the silica content in iron orthosilicate (29 wt pct) and that in iron metasilicate (45 wt pct).

The average concentrations of oxides in both slag samples obtained by EDS are listed in Table VIII. The silicate compositions of these slags are very close, which strongly suggests that the process of slag formation is completed before the over-current zone, that is the interaction between matte and slag melts is near to the

equilibrium state. Table I shows that the average values for the contents of all elements in both these slags are also very close, although one exception is the copper content. The higher copper content in the slag from the over-current zone shows that the process of sedimentation of matte reguli was not complete before the over-current zone. In addition, the slag from the over-current zone contains large matte particles (300 μm and more) while the waste slag only contains small matte reguli.

Both slags contain two types of inclusions, which were identified as magnetite and matte reguli. The regular shape of the magnetite inclusions is evidence for their precipitation during cooling of the liquid slag. By contrast, the rounded and oval shapes of the matte reguli suggest that they were in the liquid state in the slag. These inclusions determine the mechanical losses of metals in the waste slag. The chemical composition of the matte reguli in the waste slag was calculated using a similar approach to that used for the calculation of the slag inclusion composition in the matte. It is known [6] that copper does not form oxide in slag when in the contact with a sulfide melt, so that the copper observed in the slag composition is originated from the matte reguli. The ratios of the contents of all matte components to the copper content in the matte were determined from the chemical analysis data (Table I, row 1) and used to calculate their contents in the waste slag. These data are listed in Table IX (row 1). The total content of matte reguli in the slag is equal to about 0.6 wt pct, which is in good agreement with the areal measurements obtained by SEM (0.8 pct). The average chemical composition of the matte reguli was determined by normalizing the calculated data to 100 pct (Table IX, row 2). For comparison, Table IX also gives the mean composition of the matte reguli in the slag determined by EDS (row 3) and the matte composition determined by chemical analysis (row 4). There is satisfactory agreement.

C. Metal losses in slag

A major question is the partitioning of metals between oxides and sulfides when they are dissolved in slag, since zinc, lead and also iron are present in solution in the silicate melt as both oxides and sulfides. This brings us to the problem of non-ferrous metal losses in liquid waste slags.

The ionic theory of liquid slags [10] has demonstrated that all chemical compounds dissolved in slag, including sulfides, are ionically dissociated. In accordance with this idea, it was postulated that metal particles derived from MeO and MeS in the slag should be indistinguishable, since in both cases dissociation yields the same cation Me^{++} [9]. As a result, only two forms of metal losses in the slag were considered: mechanical (matte inclusions) and dissolved or electrochemical (dissolved oxides and sulfides together) [9].

However, one of the authors has shown [6] that oxides and sulfides dissolved in slag may behave differently: the sulfides of transitional metals do not necessarily dissociate in the ionic melt as discussed in [11], so that there are three different forms of metal losses: mechanical, chemical (dissolved oxides giving cations in the liquid slag) and physical (dissolved sulfides, without dissociation) [11].

Consider a heterogeneous system consisting of two homogeneous phases: liquid slag and liquid matte. Slags in non-ferrous metallurgy always contain iron oxide and the behavior of different metal compounds dissolved in the slag are determined by the chemical equilibria of the following reactions that take place in the liquid state:

$$(FeO) + (MeS) = (FeS) + (MeO), \quad (1)$$

$$(FeO) + [MeS] = [FeS] + (MeO), \quad (2)$$

$$[MeS] = (MeS), \quad (3)$$

where Me is a non-ferrous metal, the round brackets denote the homogeneous liquid slag and the square brackets denote the homogeneous liquid matte. Since the equilibrium in this complicated system is always conjugated, any shift of the equilibrium in reaction (1) to the right will also leads to a shift of the equilibrium of the heterogeneous reaction (2) to the right. Consequently, when the (MeS) concentration is low, that is dissolution of the sulfide in slag, reaction (3) practically does not proceed, and the metal is dissolved in the slag mainly in oxide form. By contrast, if the reaction (1) is shifted to the left, then sulfide is dissolved in the slag, and the equilibrium of reaction (3) is then shifted to the right. We conclude that the chemical state of non-ferrous metals dissolved in liquid slag is determined by the conjugated equilibrium of all three reactions (1), (2) and (3). The same conclusion should be true for systems where sulfur is substituted by other metalloids such as selenides, tellurides, arsenides or silisides [6].

A thermodynamic calculation for reaction (1) was made based on data given in Ref. [12, 13]. The calculation used the first approximation of Ulich's formula [14], which is justified provided that the value of the parameter M, below, is less than errors in the values of ΔH^S and ΔS^S, where ΔH^S and ΔS^S are the enthalpy and the entropy change of the reaction (1) under standard conditions. The parameter M is calculated from the relation:

$$M = \Delta c_p^S \cdot T \cdot M_o, \qquad (4)$$

where Δc_p^S is the heat capacity change for reaction (1) under standard conditions, T is the absolute temperature and $M_o = \ln(T/298) - 1 + 298/T$. The above critical conditions for using the first approximation should be met for the present case.

The slag is released from the furnace at 1300°C so this temperature was used for the calculation. However, the oxides considered are solid at this temperature

whereas they are liquid when dissolved in the slag. Therefore the latent heat of melting for the oxides and their heat capacity in the liquid state were included in the calculation.

The results of the calculation of the equilibrium constants K are given in Table X, which also lists the ratio of the equilibrium contents of sulfide and oxide derived from equation (1) for the metals in question $C_{(MeS)}/C_{(MeO)}$:

$$\frac{C_{(MeS)}}{C_{(MeO)}} = \frac{K_\gamma}{K} \cdot \frac{C_{(FeS)}}{C_{(FeO)}}, \qquad (5)$$

where $K_\gamma = \prod_i \gamma_i$ and γ_i is the activity coefficient of the component *i*. The value of $K_\gamma C_{(FeS)} / C_{(FeO)}$ was estimated to be about 0.01 [11].

For comparison, Table X also lists data calculated for cobalt, whose partition between slag and matte is well known [6, 9]: cobalt dissolves in the slag mainly in the oxide form. Zinc is similar to cobalt in its behavior and the value of $C_{(ZnS)}/C_{(ZnO)}$ should be close to that of $C_{(CoS)}/C_{(CoO)}$. As it can be seen from Table X the corresponding values are 0.12 for cobalt and 0.11 for zinc, which supports this calculation method. Lead dissolved in the slag is present mainly in the oxide form (with only 20 pct in the sulfide form). By contrast, copper is dissolved in the slag only in the sulfide form, as is known [6, 9].

These conclusions are confirmed by the present SEM/EDS results. Comparison of the total zinc content in the liquid slag (Table I, row 3) with that in the silicate portion of the slag (Table VIII) shows clearly that zinc similar to cobalt exists in the liquid slag mainly as oxide. Lead shows the same behavior. Small reguli, educed by liquation from the slag, are sulfides mainly of copper and iron; with zinc and lead present in very small quantities according to the data of Table X. The

sub-micron sulfide inclusions of oval shape differ widely in composition from the average matte composition and are evidence of the predicted physical losses. Thus, the physical losses of zinc and lead are very small, and these elements are mainly dissolved in the slag in the form of chemical losses, while copper gives only physical losses.

V. CONCLUSIONS

The slags and matte from Vanyukov's process, an autogeneous processing method of sulfide concentrates of non-ferrous metals used at the Balkhash copper-smelting plant (Kazakstan), were characterized by scanning electron microscopy, energy dispersive spectroscopy and x-ray diffraction. The following, results and conclusions were obtained:

1. The liquid matte contains 3.6 wt pct of slag inclusions and about 4 wt pct of magnetite. The solidified matte is a mixture of sulfides in which the major, matrix component was identified as geerite, $(Cu, Fe)_8S_5$. The content of copper in the matte is higher, and of iron and sulfur lower, than in mattes produced by conventional technologies.

2. The liquid waste slag contains 0.6 wt pct of matte inclusions and about 3 wt pct of magnetite. The silicate field of the solidified slag consists of two phases, which were identified as iron orthosilicate and iron metasilicate. It was proved that slag formation was essentially complete before the over-current zone.

3. The nature of metal losses with the waste slag was considered. Three forms of losses were identified: mechanical (matte inclusions in the liquid slag), chemical (metal oxides) and physical (metal sulfides dissolved in the liquid slag).

4. A thermodynamic calculation was made of the exchange reactions between oxide and sulfide components in the slag. The ratio of the sulfide and oxide forms of non-ferrous metals in the liquid slag from Vanyukov's furnace was estimated. The calculation showed that zinc and lead were present in the slag mainly as chemical losses and only partially (10-20 pct) in the form of physical losses. By contrast, copper gives only physical losses. The present experimental results support these conclusions.

ACKNOWLEDGMENTS

This research was supported under Grant No. TA-MOU-98-CA17-017 Program in U.S.-Israel Cooperative Development Research Program, Economic Growth, U.S. Agency for International Development.

Table I. Chemical analysis (wt pct) of melt products from Vanyukov's furnace

Sample	Cu	Fe^{II}	S	CaO	SiO_2	Fe_3O_4	Al_2O_3	Zn	Pb	Total measured
Matte	48.90	16.48	22.1	0.12	1.30	-	1.35	3.60	2.50	96.38
Over-current slag	3.80	30.90	1.8	2.50	31.70	2.40	5.40	6.50	1.26	94.98
Waste slag	0.31	32.40	1.9	2.90	33.80	3.20	5.10	6.30	1.20	95.05

Table II. EDS analysis of the matte

Position	Measured content of element, atomic pct											Major elements
	Fe	Cu	Zn	Pb	S	K	Ca	Ba	Si	O	Ag	
1	2.51	20.91	0.23	6.09	2.72	-	-	-	-	-	67.4	Ag-Cu
2	2.01	97.31	0.22	0.05	0.37						0.01	Cu
3	14.35	43.74	0.26	0.02	41.7	-	-	-	-	-	0.03	Cu-Fe-S
4	11.16	2.24	36.31	0.01	50.17	-	-	-	-	-	0.01	Zn-Fe-S
5	33.4	4.84	0.92	0.05	4.35	-	-	-	-	56.45	0.02	Fe-O
6	12.36	5.81	19.5	16.43	45.51	-	-	-	-	-	0.16	Cu-Fe-Zn-Pb-S
7	8.75	52.65	0.13	0.04	38.32	-	-	-	-	-	0.04	Cu-Fe-S
8	8.39	21.44	0.51	27.04	42.66	-	-	-	-	-	0.05	Pb-Cu-Fe-S
9	7.54	21.57	0.32	27.86	42.77	-	-	-	-	-	0.04	Pb-Cu-Fe-S
10	15.61	1.89	32.25	0.74	49.5	-	-	-	-	-	0.05	Zn-Fe-S
11	27.14	8.35	0.84	1.15	9.18	-	-	-	-	53.51	-	Fe-O
12	33.48	1.38	1.16	1.29	2.88	-	-	-	-	59.78	-	Fe-O
13	14.09	44.44	0.19	-	41.49	-	-	-	-	-	-	Cu-Fe-S

Table II. Continuation

Position	Measured content of element, atomic pct											Major elements
	Fe	Cu	Zn	Pb	S	K	Ca	Ba	Si	O	Ag	
14	21.52	0.58	2.01	0.07	0.62	1.42	1.97	0.32	11.29	60.2	-	Fe-Si-O
15	36.81	0.57	1.47	0.02	0.11	-	-	-	-	61.06	-	Fe-O
16	11.27	7.29	33.35	-	48.07	-	-	-	-	-	-	Zn-Fe-S
17	11.84	25.19	0.37	21.64	40.55	-	-	-	-	-	0.08	Pb-Cu-Fe-S
18	37.71	1.04	1.38	0.03	0.47	-	-	-	0.76	58.62	-	Fe-O
19	11.69	2.26	34.63	0.24	47.47	-	-	-	-	3.71	-	Zn-Fe-S
20	8.01	22.44	1.57	22.43	37.42	-	-	-	-	8.13	-	Pb-Cu-Fe-S
21	14.38	41.89	0.12	0.22	38.07	-	-	-	-	5.31	-	Cu-Fe-S
22	14.69	37.44	2.21	0.67	38.81	-	-	-	-	6.18	-	Cu-Fe-S

Table III. Average composition of major phases in the matte

Major elements	Measured content of element, atomic pct							Phase identification
	Fe	Cu	Zn	Pb	Sum of metals	S	O	
Cu-Fe-S	12.9±1.3	42.5±2.3	0.6±0.4	0.3±0.1	56.3±3.0	38.3±0.5	5.5±0.2	$(Cu, Fe)_8S_5$
Zn-Fe-S	12.1±1.0	3.3±1.2	33.2±0.9	0.2±0.07	48.8±2.0	47.5±0.4	3.7±0.1	(Zn, Fe)S
Pb-Cu-Fe-S	8.3±1.0	20.5±1.1	0.6±0.2	24.9±1.5	54.3±2.0	37.8±0.2	7.7±0.7	(Pb, Cu, Fe)S
Fe-O	35.9±0.9	1.9±0.9	1.2±0.1	-	39.0±1.5	2.0±1.0	58.7±0.9	Fe_3O_4

Table IV. Average composition of major phases in the over-current slag

Feature	Measured content of element, atomic pct											Phase identification
	Pb	Fe	Zn	Al	Mg	K	Ca	Ba	Sum of metals	Si	O	
Matrix phase (black)	0.3±0.08	8.9±0.3	2.8±0.1	4.6±0.3	0.2±0.05	0.8±0.03	3.5±0.05	0.5±0.01	21.6±0.5	18.5±0.2	58.6±0.5	Clinoferro-silite, $FeSiO_3$
Matrix phase (grey)	0.07±0.03	16.1±1.3	2.8±0.1	2.4±0.3	1.1±0.06	0.6±0.1	1.3±0.1	0.2±0.05	24.6±1.5	16.7±0.5	57.8±0.3	Fayalite magnesian, $(Fe, Mg)_2SiO_4$

Feature	Measured content of element, atomic pct										Phase identification
	Fe	Cu	Al	Mg	Ti	Cr	Zn	Pb	Sum of metals	O	
Rectangular or trapezoid grey particles	33.8±0.4	1.6±1.5	2.7±0.8	0.2±0.07	0.4±0.01	0.3±0.2	2.0±0.4	0.1±0.04	41.1±1.9	57.0±1.6	Magnetite Fe_3O_4

Table IV. Continuation

Feature	Measured content of element, atomic pct							Phase identification
	Fe	Cu	Zn	Pb	Sum of metals	S	O	
Coarse and fine oval particles	13.6±0.8	42.6±1.6	1.3±0.3	0.4±0.1	57.9±2.0	37.6±0.5	4.7±0.7	$(Cu, Fe)_8S_5$

Table V. Average composition of major phases in the waste slag

Feature	Measured content of element, atomic pct											Phase identification
	Pb	Fe	Zn	Al	Mg	K	Ca	Ba	Sum of metals	Si	O	
Matrix (black)	0.4±0.02	10.3±0.8	2.7±0.2	4.3±0.3	0.2±0.1	0.4±0.08	3.2±0.3	0.5±0.08	22.0±1.2	18.3±0.2	58.3±0.3	Clinoferro-silite, $FeSiO_3$
Matrix (grey)	0.2±0.1	14.7±0.9	2.8±0.05	2.8±0.1	1.1±0.08	0.7±0.1	1.2±0.02	0.3±0.04	23.8±1.2	16.9±0.7	58.5±0.4	Fayalite magnesian, $(Fe, Mg)_2SiO_4$

Feature	Measured content of element, atomic pct										Phase identification
	Fe	Cu	Al	Mg	Ti	Cr	Zn	Pb	Sum of metals	O	
Grey rectangular or trapezoid particles	32.2±2.0	-	3.4±0.2	0.2±0.04	0.5±0.03	0.2±0.05	2.4±0.02	-	38.9±2.2	58.4±0.4	Magnetite Fe_3O_4

Table V. Continuation

Feature	Measured content of element, atomic pct							Phase identification
	Fe	Cu	Zn	Pb	Sum of metals	S	O	
Coarse and fine oval particles	12.8±0.7	44.9±1.5	0.8±0.2	0.8±0.5	59.3±2.0	36.0±0.6	4.8±1.3	$(Cu, Fe)_8S_5$

Table VI. Composition of slag inclusions in the matte (wt pct)

Type of determination	SiO_2	FeO	Fe_3O_4	CaO	Al_2O_3	K_2O	BaO	ZnO	PbO	Total
Content in the matte	1.30	1.61	0.08	0.11	0.20	-	-	0.30	0.02	3.62
Content in slag inclusions in the matte	35.9	44.5	2.2	3.0	5.5	-	-	8.3	0.6	100
Content in slag inclusions in the matte determined by EDS	30.1	48.6	5.1	3.5	-	2.9	2.2	7.2	0.4	100
Content in the slag	33.8	41.7	3.2	2.9	5.1	-	-	7.8	1.3	95.8

Table VII. Matte composition (wt pct)

Type of determination	FeS	Cu_2S	Cu	PbS	ZnS	Total	Slag inclusions	Residue
Content in the matte excluding slag and magnetite inclusions	23.9	57.0	3.3	2.8	5.0	92.0	3.6	4.4
Content in the matte	26.0	61.9	3.6	3.1	5.4	100	-	-

Table VIII. Measured composition of silicate phases crystallized from the slag (EDS data, wt pct)

Slag sample, Phase	FeO	ZnO	PbO	MgO	Al_2O_3	K_2O	CaO	BaO	SiO_2
From over-current zone, black	25.0	8.8	2.6	0.3	9.1	1.4	7.7	3.0	43.2
From over-current zone, grey	43.1	8.5	0.5	1.7	4.5	1.1	2.7	1.1	37.4
Waste, black	28.3	8.5	3.4	0.3	8.3	0.7	6.9	2.9	42.1
Waste, grey	39.5	8.5	1.7	1.7	5.3	1.2	2.5	1.7	38.1

Table IX. Composition of matte inclusions in the slag (wt pct)

Type of determination	Cu	Fe	Zn	Pb	S	Total
Content in the slag	0.31	0.10	0.022	0.016	0.153	0.60
Content in slag inclusions	50.8	16.6	3.7	2.7	25.5	100
Content in slag inclusions determined by EDS	56.6	15.2	1.4	2.4	24.4	100
Content in the matte	53.1	16.5	3.6	2.7	24.1	100

Table X. Equilibrium parameters for the matte conversion reactions (1) at 1300°C.

Reaction	K	$C_{(MeS)}/C_{(MeO)}$
(FeO) + (CoS) = (FeS) + (CoO)	$8.2 \cdot 10^{-2}$	0.12
(FeO) + (ZnS) = (FeS) + (ZnO)	$9.3 \cdot 10^{-2}$	0.11
(FeO) + (PbS) = (FeS) + (PbO)	$4.8 \cdot 10^{-2}$	0.21
(FeO) + (Cu_2S) = (FeS) + (Cu_2O)	$2.0 \cdot 10^{-5}$	$0.5 \cdot 10^{3}$

Figure captions

Fig.1. Typical SEM micrographs obtained from the matte using back scattered electrons in compositional contrast mode. 1, 2 – metal reguli, 3, 4, 6-10, 13, 16, 17, 19-22 – sulfides, 5, 11, 12, 15, 18 – magnetite, 14 – silicate.

Fig.2. An XRD spectrum obtained from the matte sample: 1–Geerite, Cu_8S_5; 2–Sphalerite, ZnS; 3–Galena, PbS.

Fig.3. Typical SEM micrographs obtained from slag collected in the over-current zone. (Back scattered electrons using compositional contrast mode.)

Fig.4. A matte particle in the slag collected from the over-current zone. SEM image with back scattered electrons using compositional contrast mode.

Fig.5. An XRD spectrum obtained from a sample of slag collected from the over-current zone: 1-Fayalite magnesian, $(Fe, Mg)_2SiO_4$; 2-Clinoferrosilite, $FeSiO_3$; 3-Magnetite, Fe_3O_4.

Fig.6. Typical SEM micrographs obtained from the waste slag with back scattered electrons in compositional contrast mode.

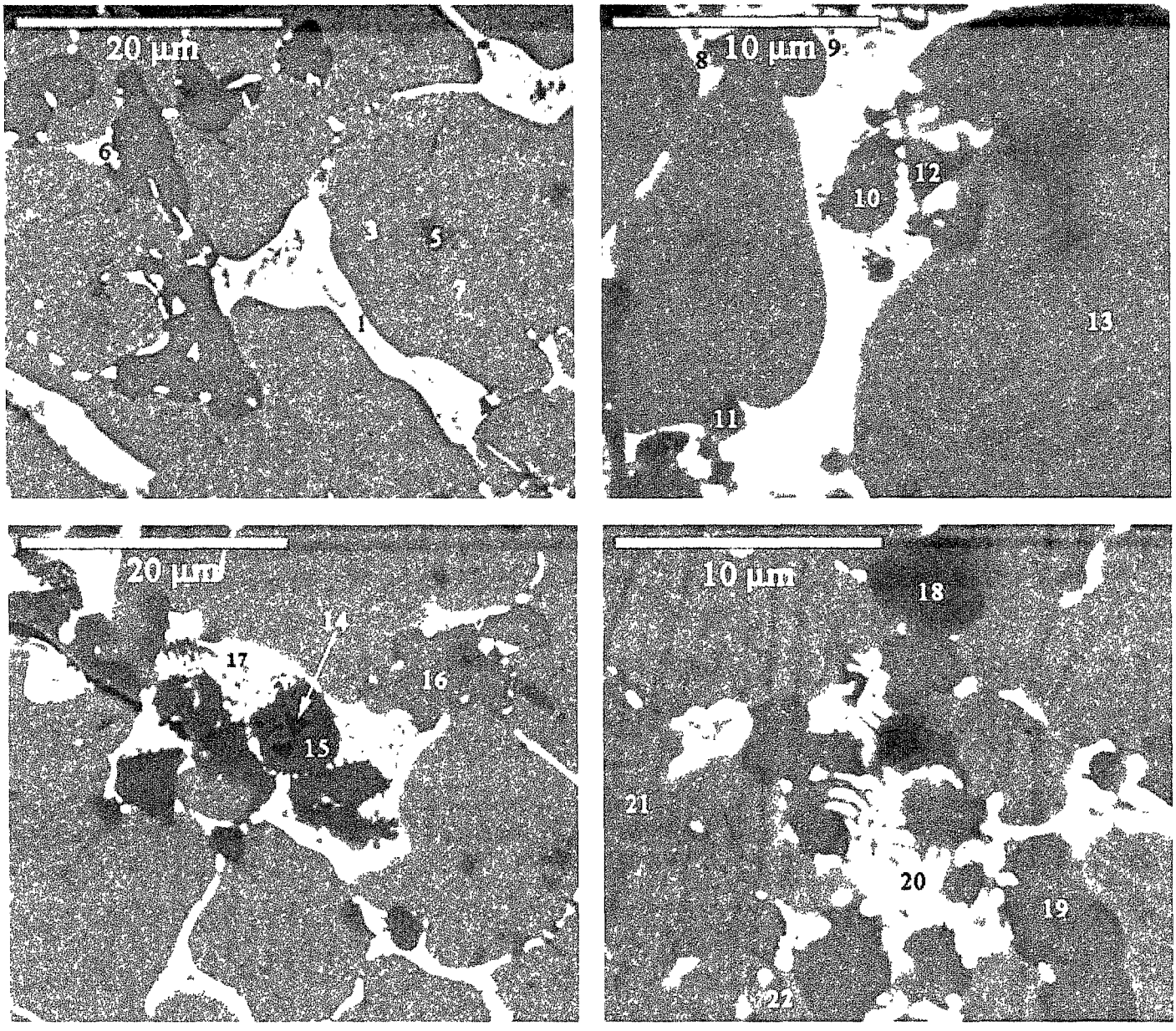

Fig.1. Typical SEM micrographs obtained from the matte using back scattered electrons in compositional contrast mode.
1, 2 - metal reguli, 3, 4, 6-10, 13, 16, 17, 19-22 - sulfides, 5, 11, 12, 15, 18 - magnetite, 14 - silicate.

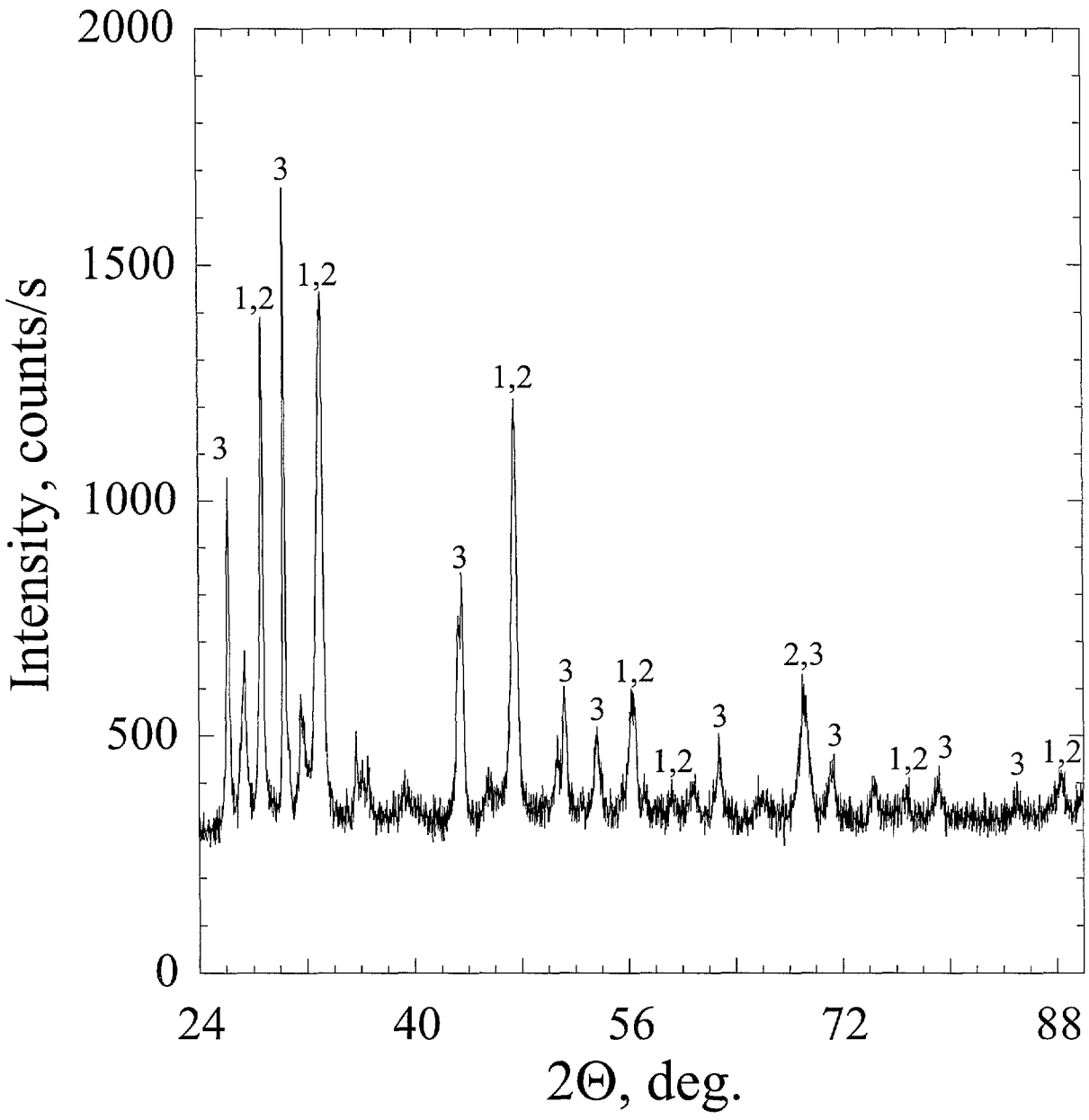

Fig.2. An XRD spectrum obtained from the matte sample:
1 - Geerite, Cu_8S_5; 2 - Sphalerite, ZnS; 3 - Galena, PbS.

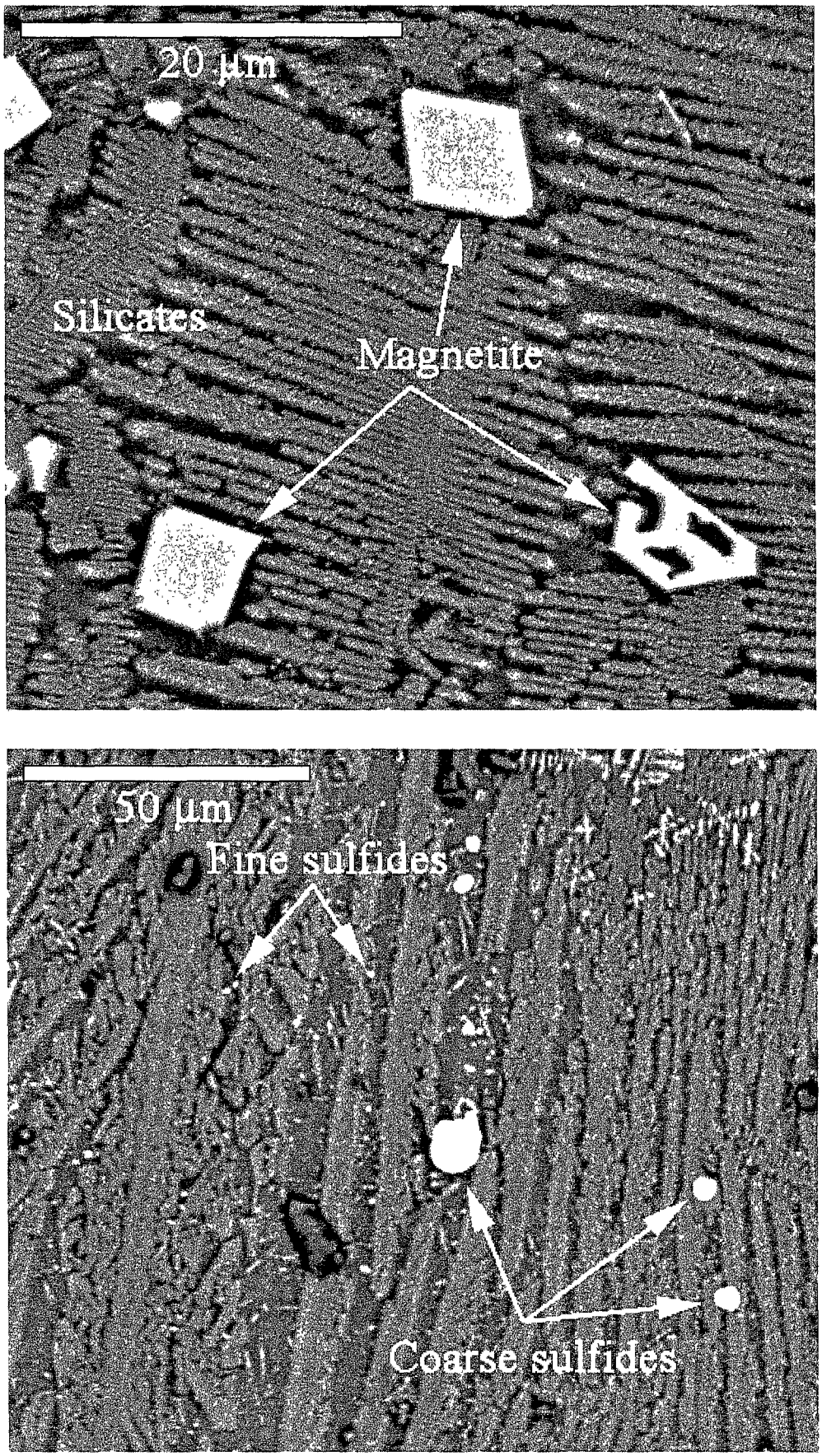

Fig.3. Typical SEM micrographs obtained from slag collected in the over-current zone (Back scattered electrons using compositional contrast mode).

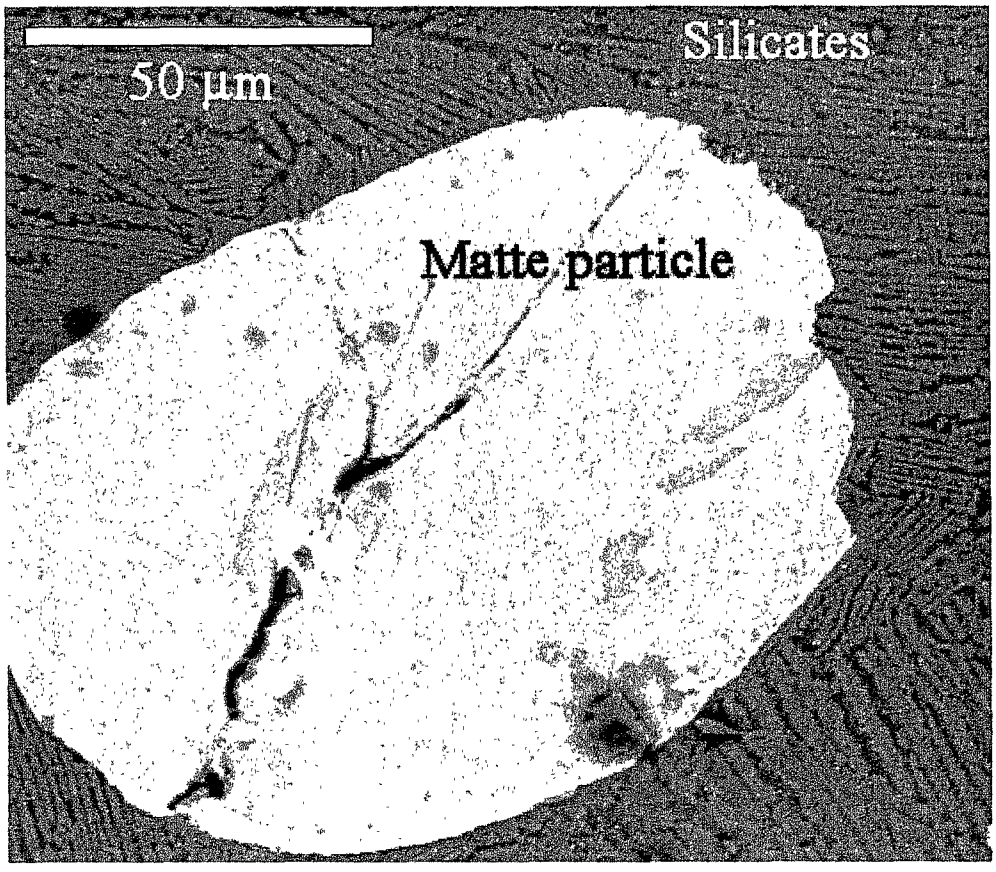

Fig.4. A matte particle in the slag collected from the over-current zone. SEM image with back scattered electrons using compositional contrast mode.

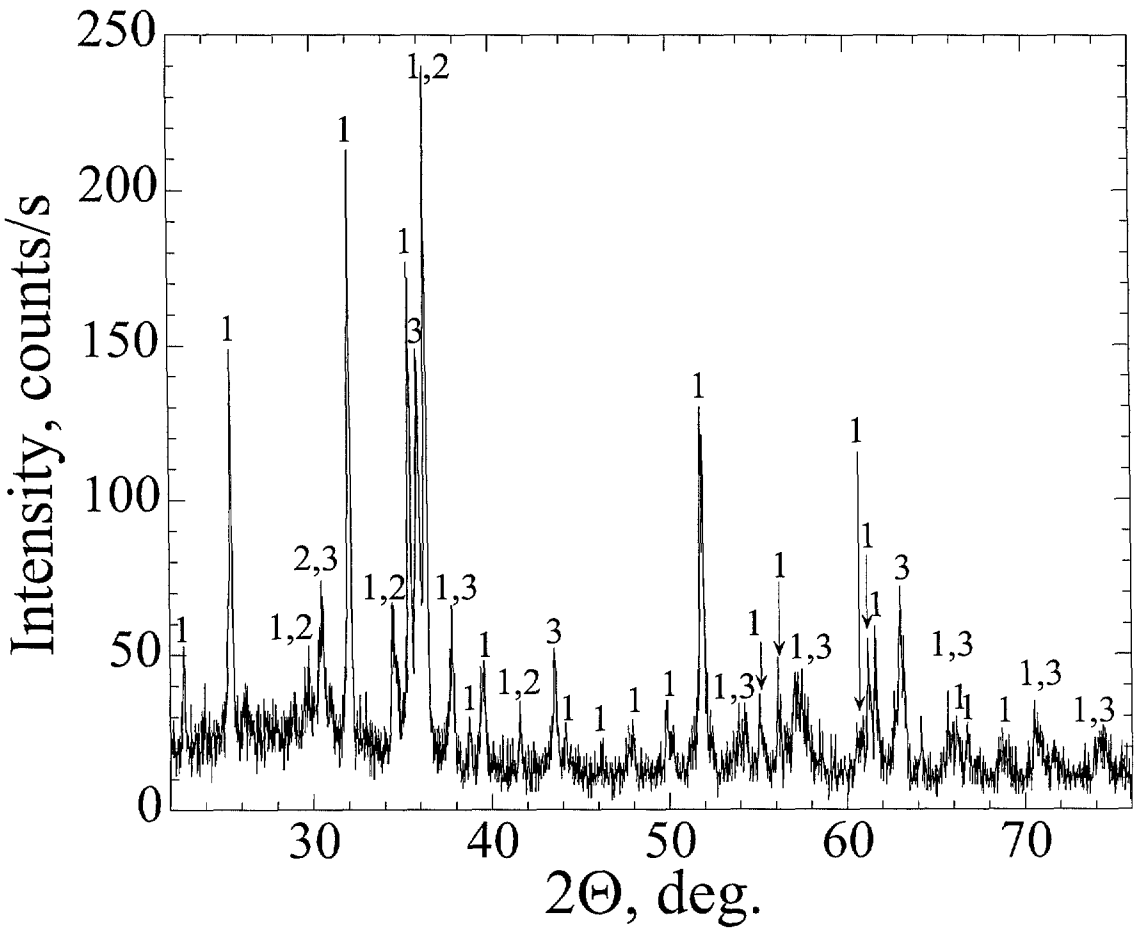

Fig.5. An XRD spectrum obtained from a sample of slag collected from the over-current zone: 1 - Fayalite magnesian, $(Fe, Mg)_2SiO_4$; 2 - Clinoferrosilite, $FeSiO_3$; 3 -Magnetite, Fe_3O_4.

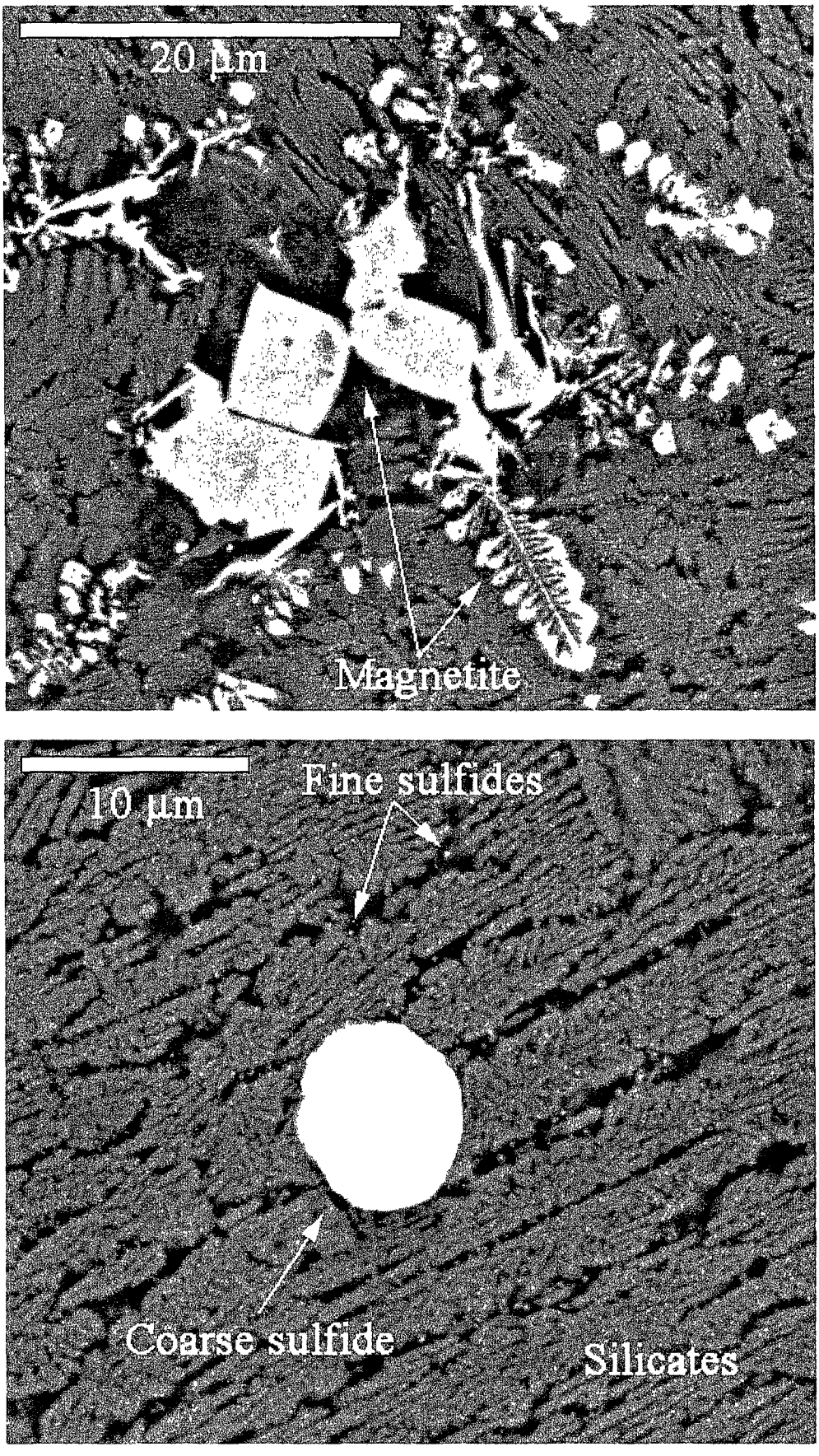

Fig.6. Typical SEM micrographs obtained from the waste slag with back scattered electrons in compositional contrast mode.

REFERENCES

1. *Smelting in Matte-Slag Liquid Emulsion*, ed. A.V. Vanyukov, "Metallurgiya", Moscow, 1988. (in Russian.).
2. V.N. Malyshev, D.I. Baiguatov, S.M. Kozhahmetov, R.Z. Zhalelev: *Proc. Int. Conf. "Environmental improvements in mineral processing and extractive metallurgy"*, Univ. Conception Press, Chili, Santiago, 1999.
3. R. Stoyanchev: *X-ray spectrometry*, 1989, vol.18, pp.165-171.
4. R. Stoyanchev, Tz. Iliev and K Recalov: : *X-ray spectrometry*, 1994, vol.23, pp.105-111.
5. *Powder Diffraction File*, JCPDS, Swarthmore, PA, U.S.A, 1990.
6. S.E. Vaisburd: *Physico-Chemical Properties and Structure Features of Sulfide Melts*, "Metallurgiya", Moscow, 1996, 304 p. (in Russian.).
7. *Binary Alloy Phase Diagrams*, ed. T.B. Massalski, 2nd ed., American Society for Metals, Metals Park, Ohio, U.S.A., 1992, pp.1467-1471.
8. A.V. Vanyukov and V.Ya. Zaytsev: *Slags and Mattes of Non-Ferrous Metallurgy*, "Metallurgiya", Moscow, 1969, 406 p. (in Russian.).
9. A.V. Vanyukov and V.Ya. Zaytsev: *Theory of Pyrometallurgical Processes*, "Metallurgiya", Moscow, 1973, 504 p. (in Russian.).
10. O.A. Yessin, P.V. Gueld: *Physical Chemistry of Pyrometallurgical Processes, part 2, Interactions with Participation of Melts*, "Metallurgiya", Moscow, 1966, 703 p. (in Russian.).
11. S.E. Vaisburd, N.N. Novikova: *Transactions of Inst. Gipronickel, Leningrad*, 1970, Vol. 46, pp. 103-110 (in Russian.).
12. O. Kubaschewski and E. Evans: *Metallurgical thermochemistry*, 3rd ed., Pergamon Press, N.Y., 1958, 426 p

13. O. Kubashevsky, C. Alcock, P. Spencer: *Materials thermochemistry*, 6th ed., Pergamon Press, Oxford, 1993, 363 p.

14. R. Wenner: *Thermochemical Calculations*, 1st ed., McGraw-Hill Book Co, N.Y., 1941, 384 p.